A&A 366, 451–465 (2001)
DOI: 10.1051/0004-6361:20000405


Astronomy & Astrophysics

# Deep submillimeter images of NGC 7331; dust at the periphery of spiral disks

P. B. Alton[1], J. Lequeux[2], S. Bianchi[3], D. Churches[1], J. Davies[1], and F. Combes[2]

[1] Department of Physics & Astronomy, University of Wales, PO Box 913, Cardiff CF2 3YB, UK
[2] DEMIRM, Observatoire de Paris, 61 avenue de l'Observatoire, 75014 Paris, France
[3] ESO, Karl-Schwarzschild-Strasse 2, 85748 Garching bei Muenchen, Germany

Received 11 September 2000 / Accepted 29 November 2000

**Abstract.** We present deep 450 and 850 $\mu$m SCUBA images of the nearby spiral galaxy NGC 7331. Using the submillimeter emissivity inferred from COBE observations of Milky Way dust, we convert our SCUBA images into maps of optical depth. The opacity derived in this way is quite low at the visible limit of NGC 7331 ($\tau_B \leq 0.22$ at the $R_{25}$ radius for the disk seen face-on). In a similar fashion, we exploit SCUBA and ISOPHOT images of a further 10 galaxies and, collectively, these data indicate $\tau_B = 0.1$–$0.2$ at the $R_{25}$ radius. Our constraints on disk opacity are fed into a simulation of how light emanating from high redshifts is attenuated by foreground spirals. In making this calculation, we consider the possibility that galactic disks may have also contained different dust masses in the past. We estimate that less than 10% of the light emitted by Hubble Deep Field galaxies fails to reach the $B$-band observer due to intervening spirals.

**Key words.** ISM: dust, extinction – ISM: molecules – galaxies: spiral – galaxies: ISM – infrared: galaxies – galaxies: NGC 7331

## 1. Introduction

Often the simplest questions in astronomy prove the most difficult to answer. Indeed, this appears to be true for galactic dust where both the quantity and distribution of interstellar grains still remains largely uncertain. In the wake of IRAS, submillimeter and millimeter imaging of cold dust (15–20 K) has revised dust masses in external spirals upwards by an order of magnitude (Guélin et al. 1993; Guélin et al. 1995; Neininger et al. 1996; Alton et al. 1998a; Siebenmorgen et al. 1999). However, the overall opacity of galactic disks still remains a contentious issue and certainly details such as the amount of interarm dust and the ultimate radial extent of galactic dust have gone unresolved.

The optical depth of spiral disks has remained controversial ever since Holmberg (1958) first addressed the problem by examining the surface brightness of disks with different inclinations (optically-thin galaxies should exhibit a higher surface brightness with increased obliqueness to the line-of-sight; Valentijn 1990; Disney et al. 1989; Davies & Burstein 1995; Block & Greenberg 1996 and references therein). This statistical test, whilst straightforward in practice, is now known to suffer from severe selection effects making interpretation very difficult (Davies et al. 1995). In the intervening years, a whole host of techniques has been applied to resolve the issue of disk opacity including: radiation transfer (Block et al. 1994; Xilouris et al. 1999), analysis of colour gradients (Corradi et al. 1996; Beckman et al. 1996; Peletier et al. 1994; Jansen et al. 1994), the occlusion of overlapping galaxies (James & Puxley 1993; White et al. 1996; Dominigue et al. 1999), the balance of FIR energy with extinguished optical energy (Trewhella 1998a; Xu & Helou 1996; Xu et al. 1997) and the systematic reddening of background galaxies viewed through nearby disks (Cuillandre et al. 2000; Gonzalez et al. 1998; Zaritsky 1994). Most of these studies indicate that galactic disks are optically-thin outside the spiral dust lane, with optical depths of $\tau_B \leq 0.4$ at the $R_{25}$ radius ($\mu_B = 25$ mag arcsec$^{-2}$ isophote). A notable exception to this is found in the work of Valentijn (1990) who maintains that optical depths closer to unity prevail at the $R_{25}$. His conclusions are based principally on the aforementioned inclination surface brightness tests, although, a more recent claim to the detection of abundant, large-scale molecular gas (using FIR spectroscopy) could, if confirmed, reinforce the idea that optically thick dust clouds exist at and beyond the disk "edge" (Valentijn & van der Werf 1999).

*Send offprint requests to*: P. B. Alton,
e-mail: paul.alton@astro.cf.ac.uk

The understanding of disk opacity is important for a large number of reasons. Galactic dust acts as a "fossil record" for previous star-formation by virtue of the fact that about half of the metals synthesized by stars end up in dust grains (Edmunds & Eales 1998; Whittet 1992). Thus, if galactic dust is shown to extend radially beyond the present-day stellar disk, this raises the issue of how such material was produced and how it attained its current location. Furthermore, it is on the surface of dust grains that molecules are believed to form (Le Bourlot et al. 1995; Williams & Taylor 1996). Thus, interstellar dust may potentially trace a component of molecular hydrogen which is too cold to have been detected in CO line studies (Lequeux et al. 1993). Historically, the most compelling reason for studying opacity has been to correct for extinction and reddening effects. Typically half of the stellar light emitted by an $L_\star$ disk is absorbed by interstellar dust (and that energy re-radiated in the far-infrared) with the result that our optical impression of external galaxies is significantly distorted (Soifer et al. 1987; Bianchi et al. 2000a). More subtly, however, disk opacity will influence our perception of distant galaxies, such as those in the Hubble Deep Field (HDF), since we effectively peer at the distant Universe through a veil of nearby galaxies (Masci & Webster 1999).

In this paper, we present deep images of the nearby Sb galaxy NGC 7331, at the wavelengths of 450 and 850 $\mu$m. The primary objective is to trace dust right up to the periphery of the optical disk (the $R_{25}$ radius). Sensitive observations of this kind are imperative because it is precisely the prevalence of any diffuse, extensive dust component (as opposed to a narrowly-confined spiral dust lane) which will determine the mean transparency of disks to light emanating from high redshifts (the peripheral and interarm regions of spirals occupy a larger filling factor in the plane of the sky). Once presented, our NGC 7331 observations will be pooled with FIR/submm images of other spirals obtained over the course of the last 4 years. Collectively these data will be used to constrain the opacity of spiral disks, the radial extent of galactic dust and the partition of grain material between arm and interarm regions. With the same goal in mind, we refer to recent investigations of systematic reddening of background galaxies viewed through M 31 conducted recently by one of us (Lequeux). Finally, we simulate the extinction of high-redshift light by intervening foreground disks. We use the opacity observed in nearby spirals to characterize the attenuation but make allowance for the evolution of optical depth with look-back time.

## 2. Submm images of NGC 7331

### 2.1. Observations

Observations were carried out during 1999 October 13–15 using the James Clerk Maxwell Telescope (JCMT) on Mauna Kea, Hawaii. The Submillimeter Common User Bolometer Array (SCUBA) is mounted at the Nasmyth focus of the telescope and provides simultaneous imaging at 450 and 850 $\mu$m for a region of sky 2.3′ in diameter (Holland et al. 1999). The shortwave array (450 $\mu$m) consists of 91 bolometers ($HPBW = 7.5''$) whilst the longwave array (850 $\mu$m) is composed of 37 elements ($HPBW = 14.7''$). In order to provide fully sampled images the secondary mirror moves in a 64-step jiggle pattern with the integration time lasting 1 s at each position. At the same time the secondary mirror chops at 7 Hz so as to remove the reference (sky) emission. After 16 steps of the jiggle pattern, the telescope nods in order to allow for slowly varying sky gradients. For NGC 7331, we used a chop throw of 3′ perpendicular to the major axis.

After each hour of observing, the telescope pointing was checked against a bright point source and skydip measurements were carried out to determine the atmospheric transparency according to elevation. The pointing was stable to better than 4″. For calibration purposes, Mars was mapped at the beginning of each night's observing and images of Uranus were taken every 2–3 hours thereafter. The SCUBA beam has moderate error lobes (especially at 450 $\mu$m) and, since NGC 7331 is an extended source, we corrected the calibration in order to take account of emission outside the central beam. The measured $HPBW$ of the central beam is 7.6″ at 450 $\mu$m and 14.9″ at 850 $\mu$m. The integrated flux density over our final maps at both wavelengths is believed to be accurate to ∼10%. However, the side-lobes associated with the beam mean that photometry over small regions of the image (e.g. 1–2 beamwidths across) are probably uncertain by 20% at 850 $\mu$m and 35% at 450 $\mu$m. For NGC 7331, and the other spirals discussed in this paper, we expect the SCUBA filters to detect primarily thermal emission from dust grains. At 850 $\mu$m, the contamination from the $^{12}$CO(3–2) emission line is estimated to be the same order as the calibration error (∼10%) for all but the very centre of these objects (Dunne 2000).

The current measurements were combined with images of the central 3′ of NGC 7331 taken by Bianchi et al. (1998) during October 1997. Although there is overlap between the two data sets, the present observations concentrate on the northern half of the disk and map the thermal dust emission to just beyond the $R_{25}$ radius (5.3′). Table 1 summarizes the exposure times and sky opacity for both observing runs. Our final sensitivity at 850 $\mu$m ($2.2 \pm 0.2$ mJy/15″ beam) is believed to represent the deepest image ever taken of a nearby galaxy in this filter.

The dedicated SCUBA software package, SURF (Jenness 1997), was used to clean, flatfield and calibrate the images according to atmospheric attenuation. SURF also facilitates a reduction in the final image noise by compensating for spatially correlated sky emission across the field of view. In common with previous authors we adopt 15 Mpc as the distance to NGC 7331. Table 2 summarizes the basic properties of the spiral galaxy NGC 7331.

**Table 1.** Submillimeter observations of NGC 7331 taken with SCUBA. Exposure times represent the total on-source integration times for each of the observing runs (October 1997 and October 1999). The final $1\sigma$ sensitivity corresponds to the northern half of the galaxy, from the nucleus up to the $R_{25}$

| | | 450 $\mu$m | 850 $\mu$m |
|---|---|---|---|
| | area mapped | $3.3' \times 5.8'$ (central disk) | |
| Oct. 1997 | exp. time | 2.5 hr | 3.2 hr |
| | mean opacity | 0.7 | 0.14 |
| | area mapped | $3.4' \times 5.5'$ (north disk) | |
| Oct. 1999 | exp. time | 6.4 hr | 6.4 hr |
| | mean opacity | 1.6 | 0.27 |
| | $1\sigma$ (final) | 6.1 mJy/7.6″ beam | 2.2 mJy/15″ beam |

**Table 2.** Basic properties of NGC 7331

| Parameter | Value | Reference |
|---|---|---|
| Type | Sb | de Vaucouleurs et al. (1991) |
| $R_{25}$ radius | $5.25'$ | ” |
| RA (J2000) | $22^{\rm h}37^{\rm m}04^{\rm s}$ | Bianchi et al. (1998) |
| Dec. (J2000) | $34°24'56''$ | ” |
| Distance | 15 Mpc | $H_0 = 75$ km s$^{-1}$(Mpc)$^{-1}$ |
| Inclination | 74° | Garcia-Gomez & Athanassoula (1991) |
| PA | 167° | ” |

### 2.2. Results

In Fig. 1, we present our final maps of NGC 7331 at 850 and 450 $\mu$m. Both images have a common spatial resolution of 17.3″ ($FWHM$) achieved, respectively, by smoothing the 850 $\mu$m image with a 450 $\mu$m beam map of Uranus and convolving the 450 $\mu$m image with the 850 $\mu$m beam map. Contours in the figure denote submm emission detected at the $2\sigma$ level or greater. As noted by Bianchi et al. (1998), the submm flux from the central $100'' \times 50''$ of the object is concentrated in a prominent ring which is known to harbour a large fraction of the molecular gas in the galaxy. This reinforces an emerging trend from submm imaging, where 850 $\mu$m emission appears to correlate spatially with the CO($J = 1 - 0$) line, a well-known tracer of $H_2$. At larger distances from the nucleus we might expect the submm emission to follow the distribution of atomic gas as $H_2$ is replaced by HI as the mass-dominant gas phase in the interstellar medium (ISM). However, profiles of the neutral gas in NGC 7331 show no obvious correlation between submm emission and HI even towards the disk edge (see Fig. 2).

We detect no significant emission close to the $R_{25}$ radius of NGC 7331 (although due to the high sensitivity of our 850 $\mu$m image we *will* be in a position to put quite tight constraints on the optical depth at the periphery of the stellar disk). Although we use a 3′ chop to sample the sky during our submm observations, the reduction of the data allows for a sizeable part of the time-correlated noise and remaining background to be removed by sampling bolometers near the array edge. The bolometers employed in this procedure lie at an equivalent distance of $1.1 \times R_{25}$ from the object centre. Thus, we feel compelled to check that no thermal emission from dust residing just beyond the $R_{25}$ radius has been inadvertently subtracted from our images when removing sky emission. Figure 3 presents azimuthally-averaged radial profiles of the 450 and 850 $\mu$m emission in NGC 7331. The latter is also shown before the final sky subtraction procedure using the outlying bolometers. Although a slight gradient is evident in the original 850 $\mu$m emission detected towards the disk edge, the profile appears to have more or less levelled out by a radius of $0.7 \times R_{25}$. Thus we believe that we are genuinely sampling the sky in the bolometers at $1.1 \times R_{25}$. Certainly, if the signal in this region is attributable in any way to the object, then the grains responsible must be distributed in a remarkably uniform fashion. The radial distribution of atomic hydrogen is generally considered to be extremely flat compared with other tracers of the ISM but the dust component in question would have to be a great deal flatter than even this (Fig. 2). For completeness, we note that the opacity associated with such a uniform dust layer, if it exists, is $\tau_B \simeq 0.5$ (based on the conversion of 850 $\mu$m flux density to optical depth carried out in the next section).

### 2.3. Conversion to optical depth

In order to infer the optical depth or amount of dust present from Fig. 1 we must have some notion of the grain temperature ($T$) and emissivity of dust at 850 $\mu$m ($Q(850\ \mu\text{m})$)[1]. Indeed, for a Galactic-type reddening law ($R_V \simeq 3$), it can be shown that the face-on $B$-band optical depth, $\tau_B$, is given by:

$$\tau_B = \frac{Q(V)}{Q(850\ \mu\text{m})} \frac{2.22\ 10^{-18}}{B(850\ \mu\text{m}, T)} \quad \cos(i) \quad f_{850} \qquad (1)$$

where $Q(V)$ is the emissivity at $\lambda = 0.55$ $\mu$m, $i$ is the inclination of the disk ($i = 90°$ for edge-on), $f_{850}$ denotes the surface brightness of the 850 $\mu$m map, in Jy/17.3″ beam, and $B(850\ \mu\text{m}, T)$ refers to the blackbody intensity at 850 $\mu$m for grains of temperature $T$ (e.g. Alton et al. 2000). This formula assumes a plane parallel geometry for the dust distribution (e.g. a slab).

Presently, we shall employ a radiative transfer simulation to derive $T$ but since the 850 $\mu$m filter operates in the Rayleigh-Jeans tail of the emission curve we do not expect $\tau_B$ to vary by more than 50% due to uncertainty in grain temperature. In contrast, $Q(850\ \mu\text{m})$ is uncertain

[1] The mass absorption coefficient ($\kappa$), which is often used, is related to the grain emissivity as follows: $\kappa_{850\ \mu\text{m}} = \frac{3Q(850\ \mu\text{m})}{4a\rho}$, where $a$ and $\rho$ are the radius and material density of the grains respectively.

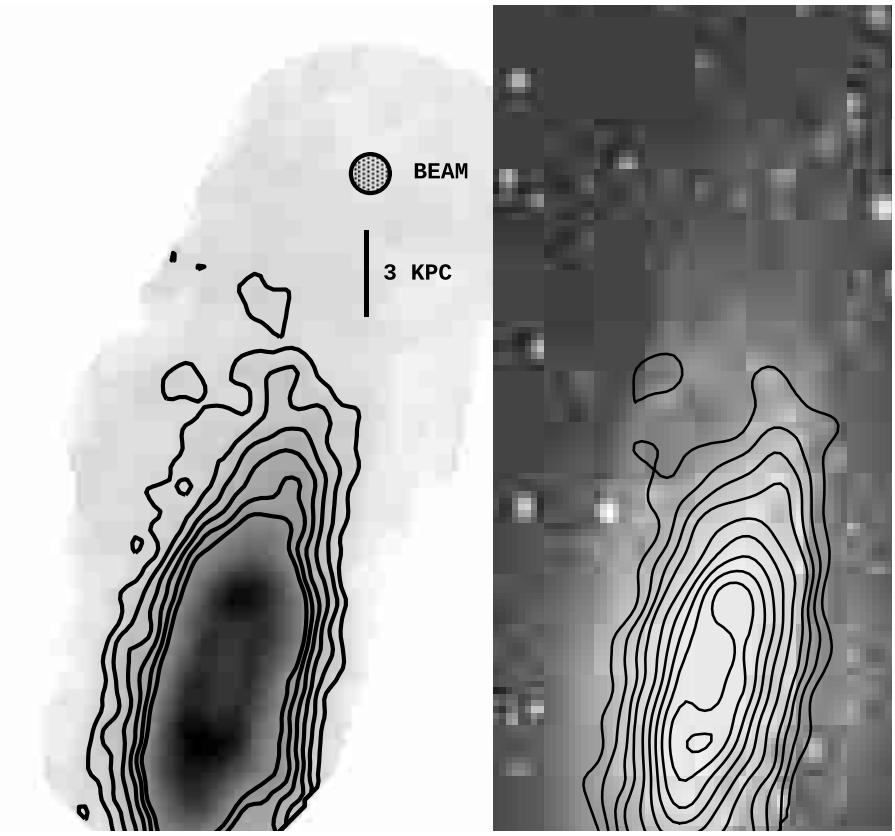


**Fig. 1.** SCUBA 850 and 450 $\mu$m maps of NGC 7331, smoothed to a common spatial resolution of 17.3″ ($FWHM$). For the 850 $\mu$m image (left), regions of lower surface brightness are traced by contours which start at $2\sigma$ (2.8 mJy/17.3″ beam) and subsequently increase by $2\sigma$. On the right, 450 $\mu$m contours have been superimposed onto a ∼2″ resolution Digital Sky Survey image ($B$-band). Isophotes begin at $2\sigma = 25$ mJy/17.3″ beam and increase by $2\sigma$ until 100 mJy/beam (thereafter the separation is $4\sigma$). Both submm maps have the same image scale and are orientated with north at the top, east to the left

by a factor of ∼3 due to a scarcity of empirical data for the emissivity of diffuse dust at long submm wavelengths. In Fig. 4 we have collated all the information currently available in the literature for $Q(\lambda)$. Near 100 $\mu$m, most measurements are based on Galactic reflection nebulae which may not typify diffuse dust residing in the ISM. The Draine & Lee (1984) model, adopted with fervour by some observers, is an extrapolation of the optical constants of carbon and silicate refractory cores in the optical and near infrared waveband into the FIR/submm regime. A correlation established by Boulanger et al. (1996) between HI column density and cool Galactic dust (COBE data), has recently provided observational data beyond 100 $\mu$m. In this case, the quantity of dust radiating in the submm is found by converting HI column density to optical depth using $E(B-V) = N_{\rm H}/5.8\ 10^{21}$ cm$^{-2}$ (Bohlin et al. 1978). Mostly recently, Alton et al. (2000) compared the *observed* 850 $\mu$m emission from the edge-on galaxy NGC 891 and related it to the optical depth inferred from a scattering+absorption radiative transfer simulation developed by Xilouris et al. (1998, 1999). This yielded a submm emissivity about a factor 3–4 higher than either the Draine & Lee (1984) and Boulanger et al. (1996) estimates. Some of this discrepancy may be attributable to *dust clumps* which are optically thin in the submm but remain poorly modelled by current radiative transfer codes.

One of the striking features of Fig. 2 is the strength of submm emission originating from the $H_2$ phase compared with the diffuse HI medium. Indeed, the HI "tail" beyond $R \simeq 0.6R_{25}$ appears to be completely unregistered by the submm curve. Although the average grain temperature is expected to fall with increasing distance from the nucleus (see below), this disparity is difficult to explain unless grains associated with the molecular phase possess significantly higher submm emissivities compared with dust in the HI environment. An enhancement of this kind might explain the factor 3 difference between $Q(850\ \mu{\rm m})$ derived by Alton et al. (2000) for the $H_2$-dominated galaxy NGC 891 and the corresponding value produced by Boulanger et al. (1996) for the HI phase of the Milky Way. Enhancements of this order have also been noted by observers of reflection nebulae and dense star-forming regions (Andre et al. 1993; Rengarajan 1984; Sopka et al. 1985; Casey 1991; see also Fig. 2) and are expected on the basis of grain conglomeration and mantle formation (Ossenkopf & Henning 1994; Mathis & Whiffen 1989). We have tested the idea that $Q$ may be higher for $H_2$ dust by comparing submm profiles of 2 other spirals

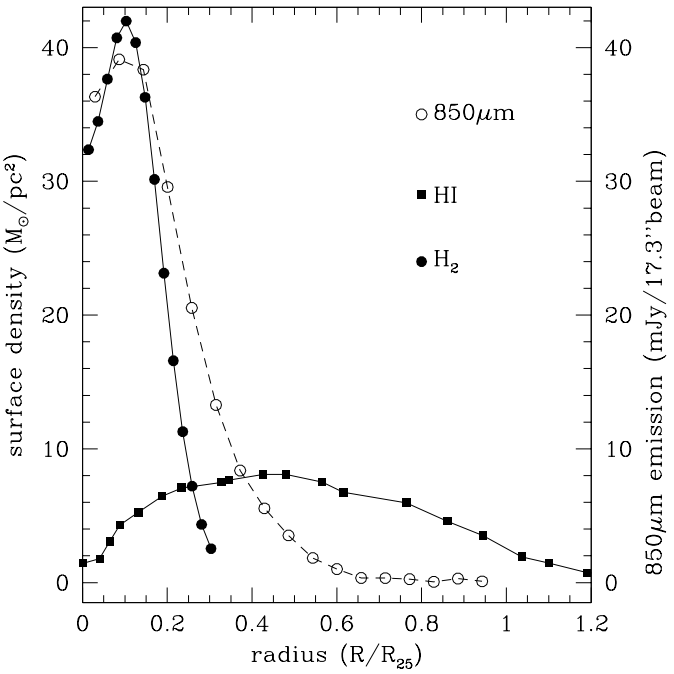


**Fig. 2.** The radial distribution of neutral gas in NGC 7331 (left axis) plotted against 850 $\mu$m dust thermal emission detected by SCUBA (right axis). The profiles have been generated by azimuthally averaging emission from the disk (although only the gas surface density has been corrected to face-on). The radius is shown as a fraction of the $R_{25}$ (315″). The $H_2$ profile was made available by the BIMA SONG consortium (Regan et al. 2000) and has been smoothed to the same resolution as the 850 $\mu$m data ($FWHM = 17.3''$). The HI profile was kindly provided by Begemann et al. (1991) and has a spatial resolution of 20″. To derive the surface density of molecular gas a value of $X = 2\ 10^{20}$ cm$^{-2}$ K km s$^{-1}$ has been assumed for the CO-to-$H_2$ conversion factor (Maloney 1990). The random errors in the 850 $\mu$m emission are comparable to the size of the markers

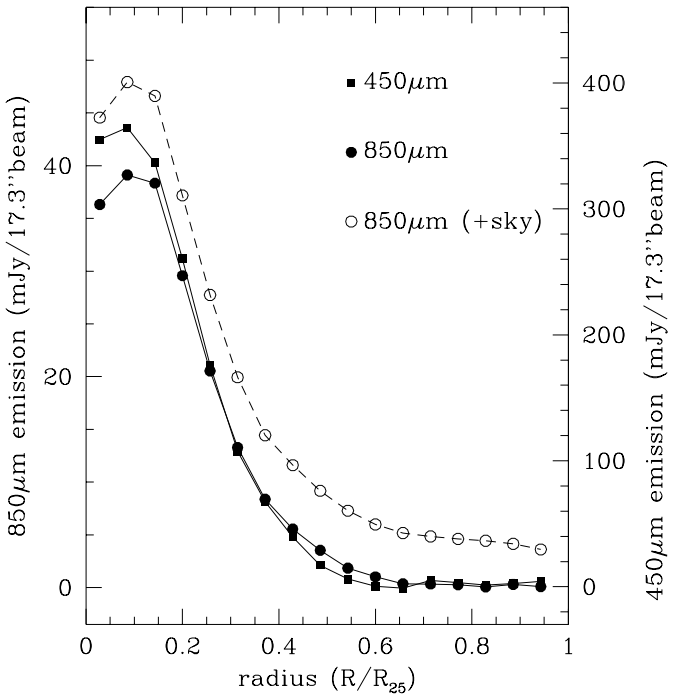


**Fig. 3.** Azimuthally-averaged radial profiles of NGC 7331 at 450 $\mu$m (right axis) and at 850 $\mu$m (left axis). The emission at 850 $\mu$m is also shown before the final sky subtraction process. The random errors in the submm emission are comparable to the size of the plotted markers

imaged with SCUBA (observations discussed below) with their corresponding HI and $H_2$ column density profiles. We were unable to confirm that $Q$ is enhanced in the $H_2$ phase, however, because our sample size is small and the emissivity of $H_2$ dust is degenerate with the CO-line conversion factor $X$ (itself uncertain by a factor of 2).

For our conversion of submm flux density to optical depth we adopt the emissivity given by Boulanger et al. (1996), namely:

$$\frac{Q(V)}{Q(850\ \mu\mathrm{m})} = 46\,000. \qquad (2)$$

Of all the current estimates of $Q(850\ \mu$m) this produces the largest value for $\tau_B$ and ultimately we wish to place upper limits on the optical depth at the periphery of spiral disks.

In order to be able to infer $\tau_B$ from Eq. (1) we still must have some notion of the grain temperature within NGC 7331. To derive this quantity we employ the radiative transfer model of Bianchi (1999). This simulation assumes smooth distributions of both stars and dust which decline exponentially with increasing galactocentric radius and height above the midplane. The light paths of photons are followed, through a succession of scattering interactions, until absorption takes place or the photon exits the galaxy. Those rays which are absorbed contribute to the heating of the dust and, in this way, a map of grain temperature can be constructed (Bianchi et al. 2000b). To simulate NGC 7331 we assumed a gas-to-dust ratio of 150 in regions of solar metallicity and a proportional decrease (increase) in this ratio for higher (lower) heavy element abundance (Issa et al. 1990). We referred to spectroscopy carried out by Oey & Kennicutt (1993) and Dutil & Roy (1999) in order to learn the O/H abundance and metallicity gradient in NGC 7331. To fix the $H_2$ column density we adopted a conversion factor of $X = 2\ 10^{20}$ cm$^{-2}$ K km s$^{-1}$ (Maloney 1990) but varying this parameter by a factor of 2 has little influence of the grain temperature eventually produced. The exponential scale-length of stars in the NGC 7331 disk was ascertained from profiling an $I$-band image obtained by Trewhella (1998b). A $r^{1/4}$ bulge component was also added to the stellar light. Colours gleaned from the literature were used to gauge the luminosity in wavebands extending from the far ultraviolet through to the $K$-band (Table 3). The exponential scale-height of disk stars, above the midplane, was fixed at 0.3 kpc and the corresponding value for the dust was set at half this value. This "sandwiching" of the main dust disk by a more vertically extensive distribution of stars is indicated by optical

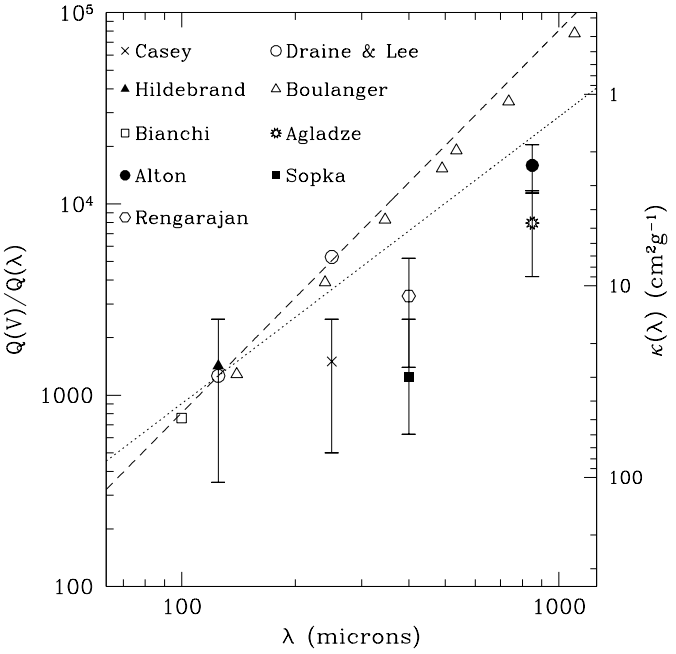


**Fig. 4.** The emissivity of dust grains in the FIR/submm waveband. Measurements are plotted for Galactic reflection nebulae (Hildebrand 1983; Casey 1991), deeply-embedded FIR sources (Rengarajan 1984), dust envelopes of evolved stars (Sopka et al. 1985) and the edge-on spiral NGC 891 (Alton et al. 2000). Agladze et al. (1994) refers to laboratory experiments conducted on silicate particulates. Draine & Lee (1984) corresponds to a model for diffuse Galactic dust partly based on empirical data. We also show values derived from COBE and IRAS data based on emission from high-lattitude Galactic dust (Boulanger et al. 1996; Bianchi et al. 1999 respectively). The dotted and dashed lines denote, respectively, $Q(\lambda) \propto \lambda^{-1.5}$ and $Q(\lambda) \propto \lambda^{-2.0}$ and are arbitrarily positioned to pass through the Draine & Lee 125 $\mu$m point. The right hand axis shows the equivalent mass absorption coefficient ($\kappa$) assuming a radius and material density of 0.1 $\mu$m and 3 g cm$^{-3}$, respectively, for the dust grains and $Q(V) = 1.5$

surface photometry of edge-on spirals (Xilouris et al. 1998, 1999).

Our simulation of dust heating in NGC 7331 indicates grain temperatures of 24 K at the centre of the object and 10 K at the $R_{25}$ radius. The temperature gradient can be approximated quite well with a monotonic fall-off with radius. Our estimate agrees well with the temperature measured for cold dust in the Milky Way (Reach et al. 1995; Masi et al. 1995) and *quiescent* spirals (Alton et al. 1998a, 1998b; Siebenmorgen et al. 1999; Israel et al. 1999; Guélin et al. 1993; Neininger et al. 1996). Galactic dust heated by the general interstellar radiation field is expected to maintain a temperature of ∼15 K (Desert et al. 1990; Mathis et al. 1983; Draine & Lee 1984) but such models for diffuse grains may not be the most suitable given that the submm thermal emission detected from NGC 7331 seems to emanate primarily from a denser molecular phase (Fig. 2). Greybody fits to the 60–850 $\mu$m thermal emission from NGC 7331 are, nevertheless, consistent with a cold ($19 \pm 2$ K) dust component, of mass

**Table 3.** Observed ultraviolet, optical and near-infrared colours of NGC 7331. We indicate the effective central wavelength ($\lambda$) and bandpass of the filter ($\Delta\lambda$). The magnitude ($M_C$) and luminosity ($L$) have been corrected for foreground attenuation by the Milky Way assuming an extinction of $A_B = 0.35$ mag (de Vaucouleurs et al. 1991). Photometry was taken from the following references: Heraudeau & Simien (1996) and Bottema (1999) for the optical wavebands; Terndrup et al. (1994) for the near-infrared; Riffato et al. (1995) for the ultraviolet filters

| Filter | $\lambda(\mu$m) | $\Delta\lambda(\mu$m) | $M_C$(mag) | $L(10^9 L_\odot)$ |
|---|---|---|---|---|
| FUV | 0.165 | 0.090 | 8.61 | 1.36 |
| MUV | 0.250 | 0.100 | 10.34 | 0.33 |
| NUV | 0.315 | 0.090 | 9.44 | 1.09 |
| $U$ | 0.365 | 0.068 | 10.21 | 1.65 |
| $B$ | 0.44 | 0.098 | 9.88 | 5.44 |
| $V$ | 0.55 | 0.089 | 9.01 | 6.05 |
| $R$ | 0.70 | 0.22 | 8.46 | 11.0 |
| $I$ | 0.90 | 0.24 | 8.03 | 8.25 |
| $J$ | 1.25 | 0.28 | 7.26 | 7.57 |
| $K$ | 2.22 | 0.42 | 6.45 | 3.23 |

$3.9 \pm 0.7\ 10^7\ M_\odot$, dominating the SCUBA filters and a warm dust component ($33 \pm 4$ K), of $3.0 \pm 2.5\ 10^6\ M_\odot$, asserting itself at short FIR wavelengths (Fig. 5). The 450-to-850 $\mu$m flux density ratio is remarkably uniform at all radii in NGC 7331 (Fig. 3) suggesting that at even near the centre of the object our SCUBA images probe cold gas clouds rather than an environment heated by recent star-formation. Indeed, the strength of the 450 $\mu$m emission compared to the 850 $\mu$m flux density is such that not only is cold dust implied but the emissivity law of the grains must also be steep ($Q \propto \lambda^{-(1.6-2.0)}$; see also Alton et al. 1998b).

Figure 6 shows the face-on optical depth inferred for NGC 7331 using the grain temperatures derived from the Bianchi simulation and the emissivity given by Boulanger et al. (1996). The azimuthally-averaged $\tau_B$ decreases from $\simeq 2.6$ in the central disk to $\leq 0.2$ at the $R_{25}$ radius.

## 3. Previous SCUBA imaging

In recent years we have acquired a sizeable number of FIR and submm observations of nearby spiral galaxies. In both this and the subsequent section we exploit this database, deriving $\tau_B$ for a sample of about 10 galaxies. We begin with SCUBA maps recently published for the edge-on galaxy NGC 891 (Alton et al. 1998b) and the face-on disk NGC 6946 (Bianchi et al. 1999).

The 450 and 850 $\mu$m emission detected from both NGC 891 and NGC 6946 correlates strongly with the presence of molecular gas. On initial inspection, the submm flux density appears fairly clumped. NGC 891 manifests a pronounced peak at the centre and secondary maxima 3 kpc either side of the nucleus (the latter purporting perhaps to a molecular ring or spiral arms viewed edge-on).

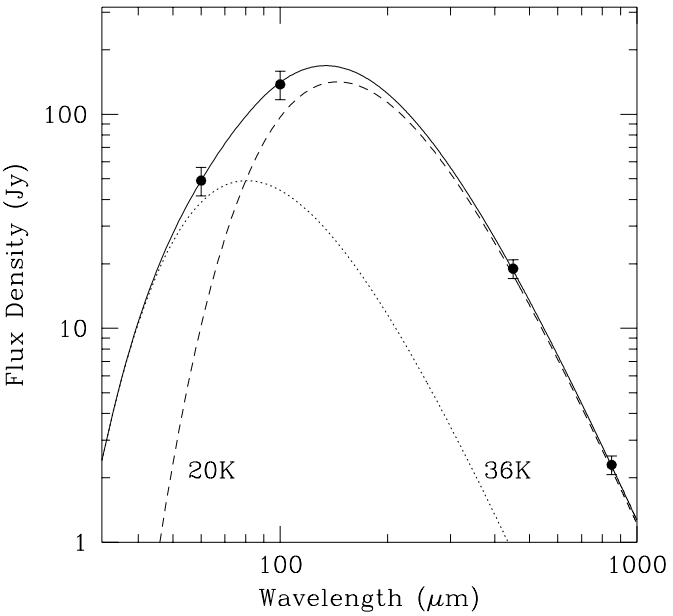


**Fig. 5.** A greybody best fit (solid line) to the FIR/submm spectral energy distribution of NGC 7331. Warm dust is traced by the dotted line whilst the cold dust component is denoted by the dashed curve. Flux densities at 60 and 100 $\mu$m have been procured from IRAS HiRes frames by integrating over the same area as the SCUBA image. For the emissivity, $Q(\lambda) \propto \lambda^{-2}$ has been assumed. Uncertainties in the spectral fit are given in the text

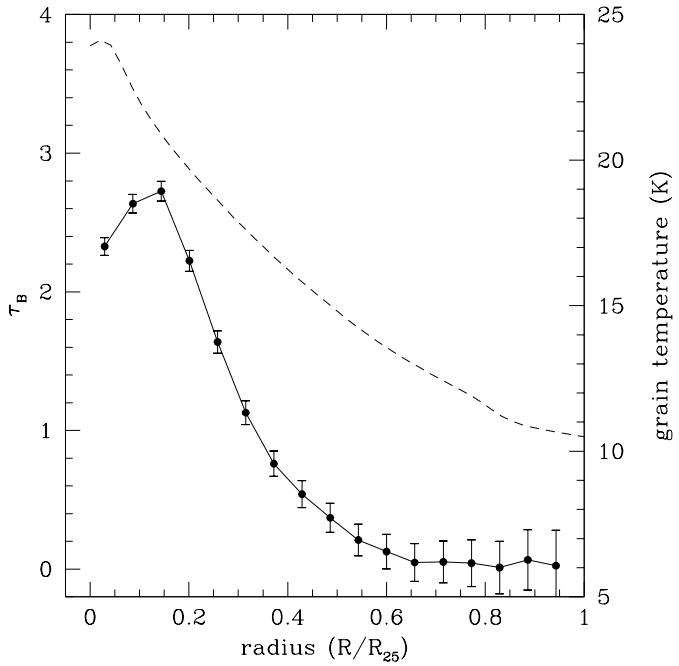


**Fig. 6.** The face-on $B$-band optical depth of NGC 7331 (left axis) inferred from submm observations. The opacity is calculated from Eqs. (1) and (2) and uses the grain temperature gauged from a radiative transfer simulation (right axis). The error bars represent the combination of random error and systematic uncertainty in the subtraction of sky emission

NGC 6946 shows greatest emission from the nucleus and the north-east quadrant of the disk. At radii $> 0.5R_{25}$, there is some evidence that the submm emission detected from NGC 891 begins to trace the *atomic* gas as it becomes the dominant phase of the ISM. Similarly, radial profiles of the gas in NGC 6946 mimic much better the shape of the submm profile if both HI and $H_2$ are considered (although, as discussed in Sect. 2.3, this depends rather sensitively on our chosen value of $X$ and $Q$ for the molecular phase). The ratio of 450-to-850 $\mu$m emission in NGC 891 is remarkably constant at all radii ($8.1 \pm 1.0$) and is consistent, as we found for NGC 7331, with cold dust dominating the optical depth and a steep form to the submm emissivity ($Q(\lambda) \propto \lambda^{(1.5-2.0)}$). In fact, greybody fits to the SCUBA and IRAS integrated flux densities reveal that 90% of the grains in NGC 891 are cold (17±3 K). Unfortunately, the 450 $\mu$m SCUBA image of NGC 6946 is not sensitive enough to allow a reliable separation of warm and cold dust.

To determine $\tau_B$, we employ once again the Monte Carlo radiative transfer code of Bianchi (1999) in order to ascertain the grain temperature. Surface photometry and UV-NIR colours are extracted from Xilouris et al. (1998) and Trewhella (1998b) for NGC 891 and NGC 6946, respectively. Once again the dust disk is modelled assuming a gas-to-dust ratio of 150 at solar metallicity (heavy element abundances from Alton et al. 2000; Vila-Costas & Edmunds 1992). The radiative transfer simulation for NGC 891 yields similar grain temperatures to NGC 7331 with a decline from 22 K at the centre to 11 K at the $R_{25}$ radius. For NGC 6946 the temperature fall-off is less dramatic – 23 K at the nucleus and 17 K at the $R_{25}$. With recourse to Eqs. (1) and (2) we produce profiles of face-on optical depth, similar to Fig. 6. Table 4 summarizes the opacity derived in this way. For the 3 galaxies which we have observed with SCUBA (NGC 891, NGC 6946 and NGC 7331) the mean, face-on optical depth is predicted to be about 0.3 or less at the $R_{25}$ radius.

**Table 4.** Opacity of nearby spirals inferred from SCUBA observations. The exponential radial scale-lengths of submm emission and $B$-band starlight are represented by $R_e(850\ \mu m)$ and $R_e(B)$ respectively. The face-on optical depth at the $R_{25}$ radius is given by $\tau_B(R_{25})$. Note that the optical depth at the edge of NGC 891 is based on an extrapolation of submm emission at shorter radii ($0.7R_{25}$) rather than an actual measurement

| Galaxy | $R_e(850\ \mu m)$ | $R_e(B)$ | $\tau_B(R_{25})$ |
|---|---|---|---|
| | ($''$) | ($''$) | |
| NGC 891 | 115 | 126 | $\leq 0.31$ |
| NGC 6946 | 103 | 145 | $0.39 \pm 0.20$ |
| NGC 7331 | 45 | 59 | $\leq 0.22$ |

The (near) face-on aspect of NGC 6946 allows us to examine the contribution of interarm dust to the overall disk opacity. This is an important consideration because the area between the spiral arms constitutes the

dominant fraction of the disk's filling factor in the plane of the sky. Thus, the overall ability of spiral disks to obscure background galaxies and light emanating from high redshifts is heavily weighted towards the opacity of such interstitial regions. We conduct aperture photometry in the north-east quadrant of NGC 6946, where the 850 $\mu$m emission is both brightest and most complete (not all parts of the disk are detected). Defining the arm region as the area where greatest $U$-band light is *observed*, we determine $18.4\pm1.2$ mJy/17.3″ beam and $15.7\pm1.1$ mJy/17.3″ beam for the arm and interarm regions respectively. Using Eqs. (1) and (2), this indicates an almost uniform opacity of $\tau_B \simeq 4$ across the star-forming locus. Furthermore, given that interarm regions subtend $\frac{4}{5}$ of the total disk face, our simple analysis suggests that as much as 80% of galactic dust is to be found between the arms (assuming a uniform temperature across the spiral wave for the cold grains). These results are surprising given that alternative studies of dust lane structure (discussed below) indicate a much greater contrast between arm and interarm localities. One potential problem is that any enhancement pattern in the submm emission may be offset from the corresponding $U$-band spiral wave. In particular, gas and dust might concentrate preferentially along the leading edge-of the density wave whereas new stars are likely to appear on the trailing edge. Under such circumstances the results from our aperture photometry would be misleading and a more thorough transect of the spiral pattern would have to be carried out using a deeper submm image fully sampling the whole disk. Fortunately, the optical depth which we derive for NGC 6946 (Table 4) is based on an *azimuthally-averaged* radial profile of the SCUBA image and, as such, should automatically sample the arm and interarm spiral regions in a properly-weighted manner. Our aperture photometry reveals that the submm emission is far less clumpy than originally supposed, indicating that diffuse dust, rather than a small number of luminous submm concentrations, will determine the average disk opacity.

Investigations into the attenuation and reddening properties of spiral dust lanes usually reveal face-on optical depths of $\tau_B = 1.5-3$ for the arms themselves and $<1$ in the interarm region. White et al. (1996) examined the surface photometry of 8 overlapping pairs of galaxies and estimated $\tau_B \simeq 1.5$ for the arm region of the foreground spiral ($R \leq \frac{1}{2}R_{25}$) and $\tau_B \simeq 0.75$ for the adjacent interarm region (see also White & Keel 1992). Berlind et al. (1997), in applying the same technique, have noted that the disk opacity inferred from $B$-band images tends to neglect dust residing in clumps. Assuming a Galactic reddening law, their recorded $K$-band attenuation, which is considered less susceptible to the clumping problem, indicates $\tau_B \simeq 3$ for the spiral arms and $\simeq 1.5$ for the interarm regions ($R \simeq 0.7R_{25}$). Gonzalez et al. (1998) have analysed the colour of background galaxies viewed through the disk of NGC 4536 (HST images) and inferred $\tau_B \simeq 1.3$ and $\leq 0.2$ for the arm and interarm respectively. These values assume a Galactic reddening law and the authors fail to specify a radius for their observations. Beckman et al. (1996) have derived $\tau_B = 2.5-3$ for the arms and $\leq 1$ for interarm regions from an analysis of colour gradients in spirals. Their technique, however, depends rather sensitively on how dust and stars are layered within the disk and assumes, rather naively, that the disk stars possess the same intrinsic colour at all radii.

We point out that Trewhella (1998a) has carried out an energy-balance procedure for NGC 6946. The optical reddening across the disk is effectively calibrated by the energy released from grain heating in the FIR (60−200 $\mu$m). Intriguingly, this method indicates that *some* of the arm-interarm contrast in optical surface brightness can be attributable to extinction by interarm dust (specifically the north-east quadrant of NGC 6946 where we have carried out submm aperture photometry). Trewhella assigns a $B$-band extinction of $\sim$1 to this interstitial region (radius $\sim 0.4R_{25}$). Unfortunately, unless the vertical layering of dust and stars is known with precision, this extinction is difficult to relate directly to $\tau_B$. However, for a typical "sandwich" geometry, whereby the dust scale-height is only half that of the stars, an optical depth of $\sim$4 is implied.

## 4. ISOPHOT observations

Over the last four years we have procured 200 $\mu$m images of 9 nearby spiral disks taken with the Infrared Space Observatory (ISO). The spatial resolution ($2'$ $FWHM$) is insufficient to resolve the spiral structure but dust masses and scale-lengths have been determined for 6 of these objects in Alton et al. (1998a; hereafter ATD). The remaining 3 galaxies were obtained in the ISO Additional Call and these are presented for the first time in Fig. 7. Our objective now is to derive the disk opacity from this reasonably large sample.

All the 200 $\mu$m data were reduced using the latest ISOPHOT interactive analysis package PIA. For those galaxies already published in ATD we found a 50% drop in the flux densities using the latest calibration files. This reduction is approximately in line with the suggestion made in ATD that early calibrations of PHOT tended to overestimate emission levels by 30%. The morphology and hence radial scale-lengths of our 200 $\mu$m images remains unaffected by the new calibration. The P32 mode, used for our observations, is believed to suffer transient and hysteresis effects after scanning a bright source such as a galactic nucleus. Consequently, one of the tasks carried out in ATD was to confirm that such detector problems did not undermine the radial scale-lengths determined from our surface photometry. The faint signal levels near the $R_{25}$ radius may be particularly adversely affected by transient effects and, consequently, we carry out one further check on the integrity of the data. Observations of one object in our sample (M 51), performed independently using the P32 and P22 mode, were accessed from the ISO data archive. The P22 mode, which does not make any use of the PHOT chopper, is believed to be far less susceptible

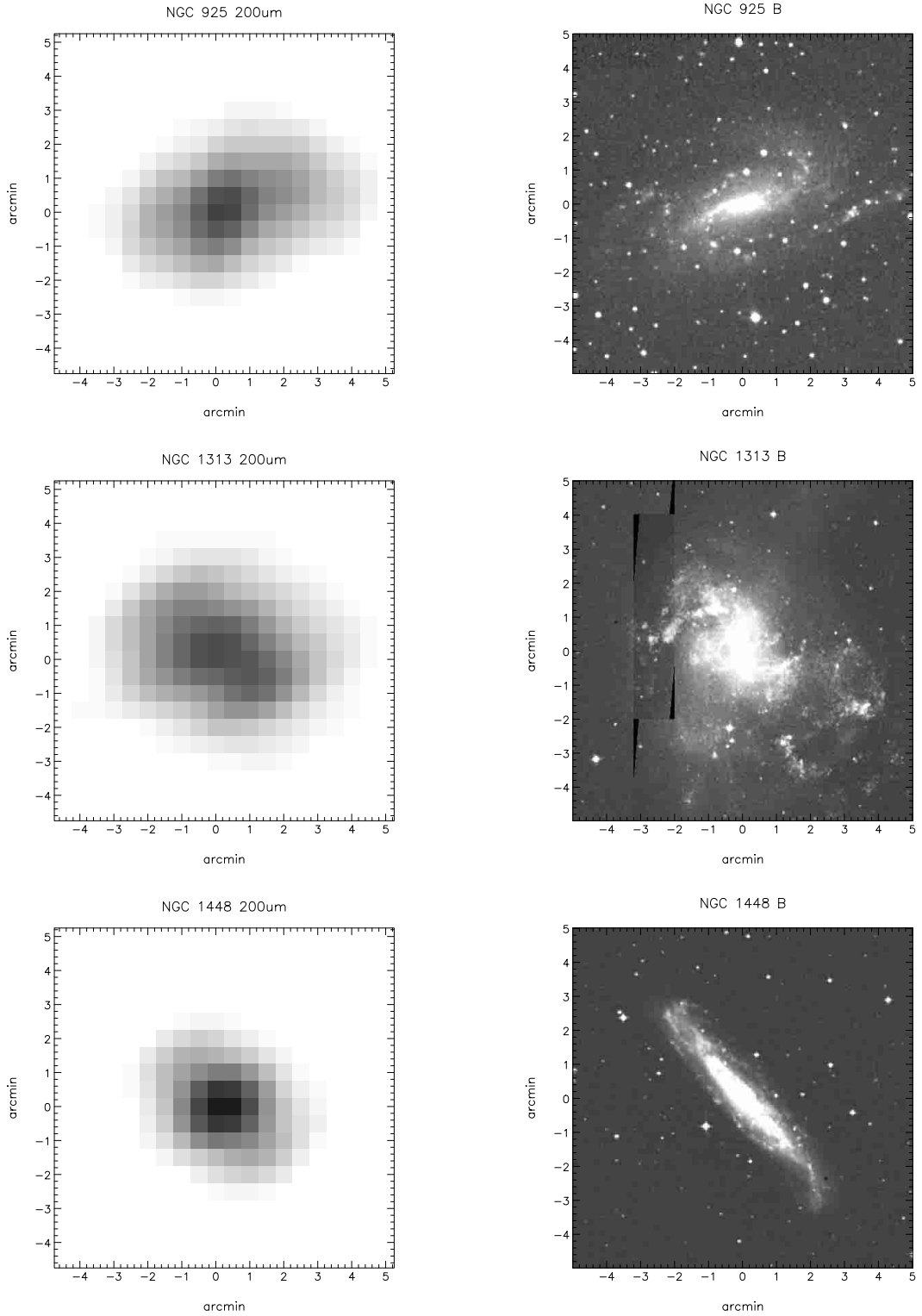


**Fig. 7.** ISOPHOT 200 $\mu$m maps of 3 nearby spirals (left) shown adjacent to the corresponding Digitized Sky Survey image ($B$-band). The spatial resolution of the FIR image is $\simeq 120''$ (as opposed to $2''$ in the optical image). The maximum surface brightness at 200 $\mu$m is 15, 18 and 27 MJy/sr for NGC 925 (top), NGC 1313 (middle) and NGC 1448 (bottom) respectively. Each panel covers an area of $10' \times 10'$ and is orientated with north at the top and east to the left

to transient effects (priv. comm. P. Richards, ISO consortium) and, as such, provides a useful comparison with the P32 mode. Reassuringly, scale-lengths derived from both sets of observations were very similar ($118 \pm 16''$ and $102 \pm 12''$ from P32 and P22 respectively).

Initially, we adopted a straightforward approach to deriving $\tau_B$ at the $R_{25}$ radius of our ISOPHOT sample. The 200 $\mu$m flux density near the disk periphery is ascertained from the PHOT image and compared with the corresponding 100 $\mu$m flux density measured from a HiRes

**Table 5.** Optical depth of nearby spirals based on ISOPHOT 200 $\mu$m and IRAS 100 $\mu$m imaging. We list the 100 and 200 $\mu$m surface brightness at the $R_{25}$ radius as $f_{100}$ and $f_{200}$ respectively. The greybody fit ($\beta = 2$) to these data is described by the grain temperature $T$ and the $B$-band optical depth ($\tau_B$). Note that the optical depth has been corrected to face-on using the disk inclination $i$. The radial scale-lengths at 100 and 200 $\mu$m are denoted by $r_{100}$ and $r_{200}$ respectively

| Galaxy | $i$ | $R_{25}$ | $f_{100}$ | $r_{100}$ | $f_{200}$ | $r_{200}$ | $T$ | $\tau_B$ |
|---|---|---|---|---|---|---|---|---|
| | (deg) | ($''$) | (MJy/sr) | ($''$) | (MJy/sr) | ($''$) | (K) | |
| NGC 134 | 71 | 243 | 2.1 | 49 | 5.8 | 83 | 16 | 0.10 |
| NGC 628 | 21 | 306 | 1.2 | 71 | 2.7 | 105 | 17 | 0.12 |
| NGC 925 | 56 | 315 | 1.2 | 102 | 2.9 | 128 | 17 | 0.07 |
| NGC 1313 | 41 | 273 | 3.2 | 82 | 3.8 | 127 | 20 | 0.07 |
| NGC 1448 | 77 | 243 | 2.5 | 53 | 2.9 | 79 | 20 | 0.02 |
| NGC 5194 | 45 | 327 | 8.7 | 70 | 10 | 104 | 20 | 0.17 |
| NGC 5236 | 24 | 336 | 9.3 | 79 | 11 | 132 | 20 | 0.24 |
| NGC 6946 | 27 | 327 | 4.9 | 82 | 12 | 158 | 17 | 0.48 |
| NGC 7331 | 69 | 315 | 1.5 | 46 | 3.0 | 86 | 17 | 0.05 |

IRAS image. A single-temperature greybody fit to the two measurements yields $\tau_B$ assuming a FIR emissivity consistent with Boulanger et al. (Eq. (2)) and $Q(\lambda) \propto \lambda^{-2.0}$ (Table 5). We were concerned that the relatively large ISO beam ($2'$) was smearing the signal radially outwards. Therefore, flux densities at the $R_{25}$ ($\sim 5'$) were also determined by extrapolating the radial fall-off between $1.5'$ and $3'$. These values were found to be within 15% of the flux densities cited in Table 5.

The single-temperature greybody fits described above take little account of either warm dust or very cold dust contributing to the 100 and 200 $\mu$m emission. To constrain the warm component we measured the 60 $\mu$m surface brightness from a HiRes IRAS image, and ascribed half of the emission to warm classical grains in thermal equilibrium with surrounding radiation field (Désert et al. 1990). This value is fitted, along with 100 $\mu$m flux density, by a warm greybody curve. The contribution of this warm dust is then subtracted from the ISOPHOT filter and the remaining 200 $\mu$m emission fitted by a dust component of 17 K (the temperature of cold grains detected in our SCUBA observations). This procedure produced optical depths that were typically $\frac{2}{3}$ the values listed in Table 5. We thus consider the single-temperature fit as providing a sound upper limit on the opacities derived for our ISOPHOT galaxies. The uncertainty in the PHOT calibration is still believed to be $\sim$30%. Therefore, the values in Table 5 are at least uncertain by this much.

## 5. Reddening studies and the dust-to-gas ratio

The final source of information on disk opacity originates from studies conducted by one of us (Lequeux) on the sytematic reddening of background galaxies and disk stars due to dust residing in the outskirts of nearby spirals. In particular, Cuillandre et al. (2000) have very recently availed themselves of the large CCD mosaic at the Canada-France-Hawaii Telescope in order to image a $28' \times 28'$ region located 23 kpc ($R = 1.3R_{25}$) from the centre of Andromeda (M 31). The authors identify a systematic $E(V-I)$ excess towards stars in M 31, which correlates spatially with the distribution of atomic hydrogen. The reddening is consistent with quite high metallicity ($\simeq$0.4 $Z_\odot$) and a $B$-band optical depth, through the inclined disk, of 0.46 beyond the $R_{25}$. Assuming an inclination of $i = 70°$ for the outer disk a value of 0.15 is indicated for $\tau_B$.

The correspondance between dust and atomic gas in the outskirts of M 31 is noteworthy because a strong correlation is known to exist between gas-phase metallicity ($Z$) and the dust-to-gas ratio ($DG$) in those galaxies close enough to have had their dust content reliably determined from extinction studies (Issa et al. 1990)[2]. Indeed, for the 6 galaxies for which Issa et al. collate metallicity and dust-to-gas values we have made a least-squares linear fit between $Z/Z_\odot$ and $DG/DG_\odot$ as follows:

$$\frac{Z}{Z_\odot} = \Big(1.42 \pm 0.22 \times \frac{DG}{DG_\odot}\Big) - 0.00 \pm 0.21. \quad (3)$$

This relationship is valid for more than an order of magnitude change in $Z$. At the same time, the constant of proportionality in Eq. (3) is so close to unity, that approximately the same fraction of heavy elements seems to be stored in grains, regardless of the metallicity of the ISM (Edmunds & Eales 1998; Whittet 1992). This leads us to believe that, given sufficient information about the metal abundance and gas content of our ISO and SCUBA galaxies we will be in a position to infer, to within a factor of 2 or so, $\tau_B$ at the disk edge. We neglect molecular gas because current evidence suggests that atomic hydrogen dominates the gas phase near the $R_{25}$ (Tacconi & Young 1986; Sofue et al. 1995). We refer to empirical data available in the literature for HI column density and measurements of $Z$ (usually from oxygen and nitrogen lines). Sometimes, however, the metallicity is inferred from the abundance gradient rather than a direct measurement. We adopt $Z/Z_\odot = DG/DG_\odot$ and $DG_\odot = \frac{1}{150}$. Table 6 shows the values of $\tau_B$ derived thus, for the 8 galaxies in our sample where gas and metallicity data are available. The opacity inferred from gas and metallicity measurements appears to be correspond closely to the values implied by submm/FIR imaging.

## 6. Opacity of spiral disks: Summary

Our conclusions from the preceding sections can be summarized as follows. We have used a variety of techniques to infer the $B$-band opacity of nearby galactic disks (our

[2] In this section, we refer to the *dust-to-gas* ratio rather than the *gas-to-dust* ratio when addressing the relationship between gas and dust. It is the former which correlates positively with metallicity.

**Table 6.** Opacity of SCUBA/ISO galaxies, at their $R_{25}$ radius, inferred from HI column density and gas-phase heavy element abundance. Column (2) gives the metallicity with respect to solar and Col. (3) lists the observed column density of atomic gas. The face-on optical depth at the $R_{25}$ radius, $\tau_B$, is calculated from Eq. (3) using the inclinations given in Table 5. References for $Z$ and $N_{\rm HI}$ are as follows: (1) Kamphuis & Briggs (1992); (2) Shostak et al. (1984); (3) Vila-Costas & Edmunds (1992); (4) Wevers et al. (1986); (5) Dutil & Roy (1999); (6) Alton et al. (2000); (7) Ryder et al. (1995); (8) Bosma (1981); (9) Tilanus & Allen (1991); (10) Rots et al. (1990); (11) Tilanus & Allen (1993); (12) Tacconi & Young (1986); (13) Boulanger & Viallefond (1992); (14) Zaritsky et al. (1994); (15) Begeman et al. (1991)

| Galaxy | $\frac{Z}{Z_\odot}$ | $N_{\rm HI}$ ($10^{20}$ atoms/cm$^2$) | $\tau_B$ | References |
|---|---|---|---|---|
| NGC 628 | 0.19 | 5.8 | 0.07 | 1, 2, 3 |
| NGC 925 | 0.29 | 7.3 | 0.07 | 4, 5 |
| NGC 891 | 0.33 | 2.2 | 0.05 | 6 |
| NGC 1313 | 0.26 | 7.5 | 0.08 | 3, 7 |
| NGC 5194 | 0.76 | 0.9 | 0.04 | 8, 9, 10, 3 |
| NGC 5236 | 0.85 | 2.2 | 0.12 | 11, 3 |
| NGC 6946 | 0.60 | 6.2 | 0.24 | 12, 13, 3, 14 |
| NGC 7331 | 0.55 | 3.4 | 0.12 | 8, 15, 5 |

sample spans a range of spiral types). The partitioning of dust between arm and interarm regions remains uncertain and can only be addressed with deeper submm images of face-on disks. However, by means of azimuthally-averaged radial profiles, we have established a mean face-on optical depth, at the $R_{25}$ radius, of $\overline{\tau_B} \leq 0.31$ from 850 $\mu$m SCUBA images of 3 galaxies and $\overline{\tau_B} = 0.15$ from 200 $\mu$m ISO images of 9 galaxies. Detections of reddening by dust at the $R_{25}$ radius of 2 spirals yielded $\overline{\tau_B} = 0.19$ and analysis of the gas phase metallicity for the galaxies observed with ISO and SCUBA indicates $\overline{\tau_B} = 0.099$. *We conclude that the B-band face-on optical depth at the $R_{25}$ radius lies somewhere between 0.1 and 0.2.*

Our results give little support to the idea that galactic disks are optically thick at the $R_{25}$ radius (Valentijn 1990; Valentijn & van der Werf 1999). Our mean values for $\tau_B$ agree fairly well with other (recent) estimates. The surface photometry of overlapping galaxies generally indicates 0.2–0.4 at the $R_{25}$ distance (White et al. 1996) although the $K$-band study of Berlind et al. (1997) is more suggestive of $\tau_B = 0.5{-}1.0$ near the disk edge. Xilouris et al. (1999) have simulated the surface photometry of 7 near edge-on galaxies, using a scattering+absorption radiative transfer model. Their results, corroborated independently across several wavebands from $B$ to $K$, indicate a very low face-on opacity at the $R_{25}$ radius ($\tau_B = 0.06 \pm 0.03$). Our exploitation, in the current study, of a diversity of techniques should mitigate against any tendancies to systematically over- or underestimate the optical depth. For example, the mean optical colour of background galaxies viewed the outskirts of a foreground spiral disks might be expected to be rather insensitive to dust clumps. However, such concentrations of material will remain optically thin at FIR and submm wavelengths and should not, therefore, be missed in our ISO and SCUBA images.

When discussing the ability of foreground disks to block the light from high redshifts (Sect. 7) we shall require a determination of the opacity *scale-length*. An extension of the techniques introduced in the previous sections allowed us to derive, respectively, $\overline{\tau_B} = 5.1$ (s.d. = 2.3) and $\overline{\tau_B} = 0.62$ (s.d. = 0.75) for the average *central* optical depth of our SCUBA and ISO objects. By corollary, the average radial scale-lengths are 127″ (s.d. = 14″) and 267″ (s.d. = 138″), respectively. In contrast to the determination of $\tau_B$ near the disk edge, the 850 and 200 $\mu$m observations indicate quite different central opacities. It seems likely that the relatively large beamwidth of the ISOPHOT instrument (117″) is responsible for the lower optical depths inferred from the 200 $\mu$m images. We have tested this hypothesis by smoothing our SCUBA images to 117″ resolution and discovered, thereby, a factor 2–3 reduction in the implied central opacity. Other studies of disk opacity imply 1.5–3 along the spiral arms (Sect. 6) and, therefore, we would expect $\tau_B > 3$ at the nucleus unless the central gas reservoir has been consumed by intense star-formation (Young & Scoville 1982; Tosaki & Shioya 1997). In contrast, radiative transfer simulations of edge-on spirals indicate face-on optical depths of only $\simeq$0.7 at the nucleus (Xilouris et al. 1999). We conclude that $\tau_B \sim 3$ at the centre of spiral disks but we recognize that there is considerable uncertainty in this value ($\pm$2). For $\tau_B = 3$ at $R = 0$ and $\tau_B = 0.2$ at $R = R_{25}$, we infer an exponential scale-length of 5.6 kpc ($\overline{R_{25}} = 15.3$ kpc for the galaxies we have observed with ISO and SCUBA).

Finally, for a complete definition of disk opacity, the maximum radial extent of galactic dust should be established. Currently, there are few direct measurements of how far out dust can be found from the disk centre. If grains continue to follow the distribution of atomic gas beyond the stellar disk, as appears to be the case for M 31 (Sect. 5), the maximum radial extent of the dust might coincide with the edge of the HI plateau. Krumm & Salpeter (1979) have found that the size of the HI disk (defined as $N$(HI) > 1.1 $10^{20}$ atoms/cm$^2$) is approximately equal to the Holmberg diameter ($\simeq 1.4 \times D_{25}$) for a large range of spiral types. Thus, even if the metallicity gradient is rather flat beyond the edge of the stellar disk (Kaufer et al. 1994), on the basis of Eq. (3) we can expect no more than $\tau_B \sim 0.01$ beyond $1.4R_{25}$. Zaritsky (1994) claims to have detected dust at galactic radii of 60 kpc (3–4 $\times R_{25}$) via the systematic reddening of background galaxies viewed through the halos of two nearby spirals. This detection is only marginally significant at the $2\sigma$ level and evidence for such extensive dust halos has *not* been forthcoming from similar reddening studies conducted by

Lequeux et al. (1995). The Zaritsky result, if confirmed, is incompatible with a straightforward radial extrapolation of our ISO/SCUBA opacity and would imply a considerable flattening in the dust distribution beyond the optical disk (see also Nelson et al. 1998).

## 7. Attenuation of light from high redshifts

Part of the motivation for examining the opacity of spiral disks is that we view the distant Universe through, what amounts to, a foreground screen or "veil" of much closer galaxies. This has the effect of both *attenuating* and *reddening* light emitted by high redshift systems before it can be recorded by the observer (Heisler & Ostriker 1988; Fall & Pei 1993; Masci & Webster 1999). In this section, we begin to assess the magnitude of this effect on the basis of the opacity we have just derived for nearby spirals. One key result is a prediction of foreground extinction to Hubble Deep Field galaxies (HDF; Madau et al. 1996).

### 7.1. Calculation parameters

A procedure for estimating the fraction of high-redshift light blocked by foreground disks has already been presented in Alton et al. (2000). In the current treatment, however, we use much more robust estimates for the disk opacity and we allow for the fact that the optical depth of the intervening spirals will itself evolve with increasing look-back time. In the first instance, our simulation assumes a Universe populated with disks similar to those investigated in the preceding sections. Initially, our calculation only considers field spirals distributed with a density of $n_0 \simeq 0.01$ per Mpc$^3$ (Loveday et al. 1992). For each slice in redshift, the real density of spiral galaxies is calculated and, accordingly, their contribution to the optical depth at that redshift is determined. Finally, we compute a covering factor, $f$, which is defined as the fraction of light emitted at redshift $z$ which fails to reach a $B$-band observer due to the sum of intervening disks. The fraction of light, $\mathrm{d}f$, lost from each slice in redshift, $\mathrm{d}z$, is given as follows:

$$\mathrm{d}f(z) = \Big(1 - \int_{z=z+\mathrm{d}z}^{z=\infty} \mathrm{d}f(z)\Big) \int_{R=0}^{\infty} 2\pi\sqrt{\sin(57^\circ)} \times R(1 - \mathrm{e}^{-\tau_B(R,z)})\mathrm{d}R \quad n(z)\mathrm{d}z \qquad (4)$$

where the redshift-dependent real density, $n(z)$, for a Friedmann Universe takes the form of:

$$n(z) = \frac{n_0 c}{H_0}\Big(\frac{(1+z)}{(2qz+1)^{\frac{1}{2}}}\Big). \qquad (5)$$

(Here, $c$ is the velocity of light, $q$ the deceleration parameter and $H_0$ is the Hubble constant).

Essentially, Eq. (4) can be understood as the fraction of light unattenuated at higher redshifts (first integral) multiplied by a "disk integral" corresponding to the optical depth at the given redshift $z$ (second integral). It should be noted that the disk integral depends not only on the optical depth at each radial position $R$ in the disk but also on the redshift at which the absorber is located. Light received in the $B$-band, by the observer, has been attenuated by the UV–FUV part of the extinction curve at higher redshifts and $\tau$, consequently, assumes a redshift dependency in our calculations. Throughout the computation we adopt a Galactic reddening law for the $\tau$ dependency on $z$. Our solutions are somewhat sensitive to the precise behaviour of reddening in the UV regime (e.g. Galactic or LMC-type extinction law). However, for the redshifts of interest ($z < 3$), such differences are negligible. For more detail concerning our computation of $f$ we refer to Trewhella (1998b) and Heisler & Ostriker (1988) which adopt a similar approach to the current method.

For the disk opacity, the critical parameters are: the radial scale-length of the dust ($R_\mathrm{e}$); the maximum radial extent of the grain material ($R_\mathrm{max}$); and the overall level of optical depth (defined by $\tau_B$ at the $R_{25}$ radius). These quantities are taken from Sect. 6 which summarizes our observational results. Thus, we adopt $R_\mathrm{e} = 5.6$ kpc, $R_\mathrm{max} = 1.5R_{25} = 23$ kpc and $\tau_B = 0.2$ at the $R_{25}$ radius. There is considerable uncertainty in the optical depth at the centre of spiral disks and hence the dust scale-length (Sect. 6). However, the covering factors that we will compute are only slightly affected (of order 10%) by these variations. It is primarily dust in the outer disk which is most liable to block background light and this is well constrained by our observations. As discussed previously, we expect the optical depth to be very low beyond $\simeq 1.5R_{25}$. However, given the aforementioned importance of the peripheral regions, we test the influence of dust extending beyond $1.5R_{25}$ on our calculations. Briggs et al. (1980) have found that most spirals have $N(\mathrm{HI}) < 3\ 10^{18}$ atoms/cm$^2$ at $R \simeq 3.4R_{25}$ although a small fraction possess column densities closer to $\sim 10^{19}$ atoms/cm$^2$. Assuming, conservatively, a gas-phase metallicity of $Z = 0.5 \times Z_\odot$ in these outer reaches, then $\tau_B$ is likely to be $\sim 0.003$ if the dust still remains coupled to the atomic gas. Adding a plateau of dust with $\tau_B = 0.003$ from $1.5R_{25}$ to $3.4R_{25}$ produces negligible changes to our results. Accordingly, we adopt $R_\mathrm{max} = 1.5R_{25} = 23$ kpc hereafter. The face-on optical depth of the foreground disks in our attenuation calculation can be summarized as follows:

$$\tau_B(R) = 3\mathrm{e}^{-\frac{R}{5.6}} \qquad (6)$$

for radii $0 \geq R \geq 23$ (kpc) and $\tau_B(R) = 0$ for $R > 23$ kpc.

Since a large number of the foreground disks included in our calculation are themselves located at high redshift, we consider the change in disk opacity expected with look-back time. One of us (Churches 1999) has recently examined the evolution of disk opacity in detail (see also Churches et al. 2000). The conclusions of Churches are based on a SPH-Treecode numerical simulation of the monolithic collapse of a gas cloud into a spiral disk. The gas is surrounded by a spherical dark matter halo which constitutes 90% of the total mass of the system. The gas cloud is described by an initial spin and star-formation is

allowed to proceed according to a Schmidt law (i.e. star-formation rate per unit disk area $\propto \rho^{1.5}$ where $\rho$ is the gas density). At specified time intervals, radial profiles of gas-phase metallicity, $Z$, and gas column density, $N$(H), can be produced from the simulation. We have used this information to infer the time-dependent disk opacity assuming that the dust-to-gas ratio ($DG$) scales as $Z$ so that $DG = \frac{1}{150}$ at $Z = Z_\odot$ (Sect. 5). The SPH code is regulated by a small number of parameters but we set the initial conditions so that a baryonic disk of roughly 1.5 $10^{11}$ $M_\odot$ forms within a distance of 10 kpc from the centre of mass (equivalent to the mass enclosed by the solar circle). We also stipulate a proportionality constant for the Schmidt law such that 90% of the initial gas mass is converted into stars after 5 Gyr (approximating the star-formation history of the Galaxy). The results from our simulation are shown in Fig. 8. The central optical depth and the scale-length of disk opacity are predicted for a 5 Gyr period.

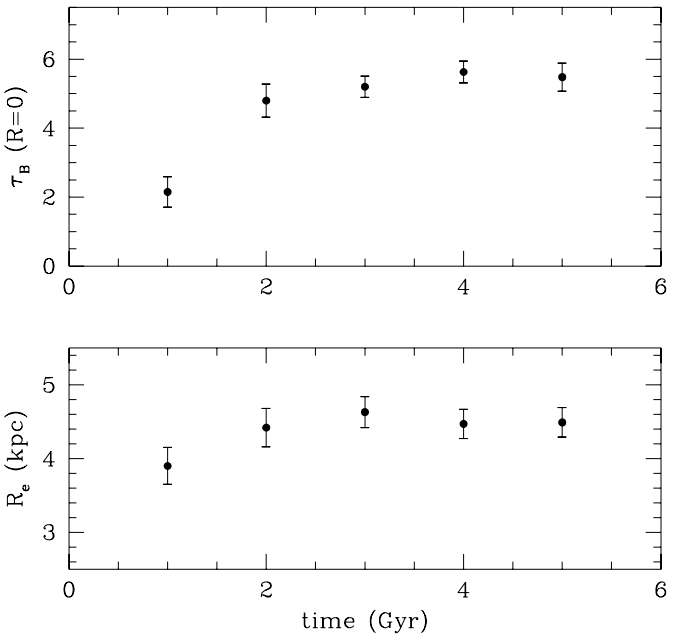


**Fig. 8.** The evolution of disk opacity according to a SPH-Treecode numerical simulation. Markers trace the face-on central optical depth, $\tau_B(R = 0)$, and the exponential radial scale-length of galactic dust, $R_e$, with time. Given the limited number of simulation trials (3), errorbars are used to denote the poisson noise in the values

Figure 8 predicts an increase in central optical depth and dust scale-length over the first 2 Gyr of the disk evolution but little change in disk opacity thereafter. These results are somewhat surprising given that Edmunds & Eales (1998), addressing the same physics analytically, find that present-day spirals may have had dust masses 50–100% higher *at certain times* in the past. Maximum dust masses may be expected to occur, according to these authors, when the gas fraction is close to half. Prior to this, the heavy elements required to form dust are still building up in the ISM via star-formation. As the mass in stars begins to overtake the mass present in gas, metals tend to become locked up in stellar cores and the dust mass starts to decline. The reason why the SPH simulation of Churches fails to show a discernible downturn in opacity is because we do not monitor the disk evolution to sufficiently low gas fractions.

Clearly, the relationship between the evolution of disk opacity and redshift depends on the adopted cosmological model and the epoch at which spirals are believed to form. For what immediately follows, we assume spirals formed at $z \simeq 3$ and we live in a Einstein-de Sitter Universe ($q = \frac{1}{2}$). We recognize that deep Hubble images may indicate that spirals assembled much closer to $z = 2$ (Pascarelle et al. 1996; Abraham et al. 1996; Driver et al. 1998) and, therefore, our results for redshifts higher than about 2 should be treated with caution. We allow the dust mass in the foreground disk to change with time according to the analytical predictions of Edmunds & Eales. This is done by increasing the central opacity by the corresponding amount but maintaining a constant radial scale-length for the dust (the latter suggested by our SPH simulation). In experimenting this way, we find that the covering factors derived from our high-$z$ attenuation simulation change by only $\simeq$13% compared with an unevolving dust mass model. This is not a significant amount given the low covering factors that we will derive below.

### 7.2. Calculation results

Figure 9 shows the predicted attenuation by foreground disks assuming Eq. (6) at all redshifts, a zero cosmological constant, $H_0 = 75$ km s$^{-1}$ Mpc$^{-1}$ and a value of either 0 or 0.5 for $q$. Although we show the covering factor up to $z = 4$, the relevance of our model for $z > 3$ is doubtful given that spirals may not have had time to form by then. For galaxies detected in the Hubble Deep Field (assuming typically $z = 1{-}2$ here), less than 10% of the light appears to be lost according to our simulation. Heisler & Ostriker (1988) predict a much more severe attenuation by foreground objects compared with the present study. This is because they adopt a dust scale-length of 33 kpc for their absorbers – a radial size which is too large to be reasonably ascribed to spiral disks. We derive very similar levels of attenuation to Heisler & Ostriker if we adopt their parametrization of opacity for the absorbers.

The calculations thus far take no account of the propensity of many spirals to group into clusters and that line-of-sights through such concentrations of galaxies may be subject to much higher levels of attenuation. A proper examination of such effects would require inclusion of the correlation function of galaxies and a description of large-scale structure in our computation. To gauge the size of such effects we have calculated the opacity of various lines of sight through the nearby Virgo cluster. Sandage et al. (1985) classify 180 cluster spirals of type Sa $\rightarrow$ Sd within a radius of 6° (2 Mpc) of the Virgo centre. Clearly, there will be a whole range of optical depths through the cluster according to how the light path intercepts the cluster

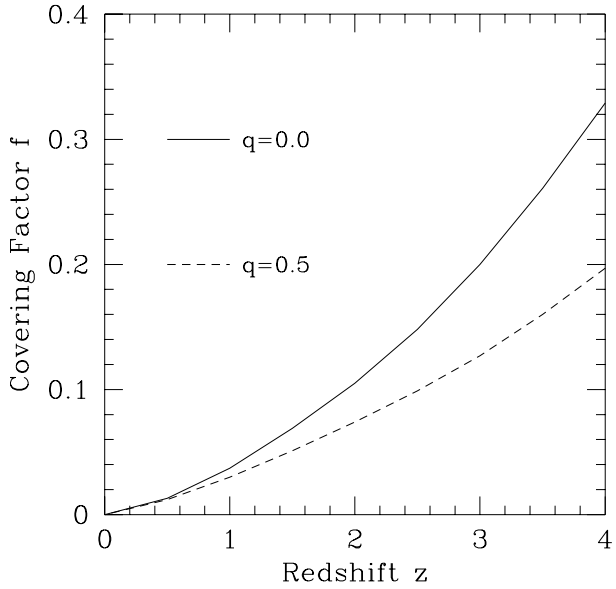


**Fig. 9.** The fraction of light, $f$, emitted at redshift $z$ which fails to reach the $B$-band observer due to attenuation by foreground spiral disks. We show results for an open (solid line) and flat Universe (dashed line) with zero cosmological constant and $H_0 = 75$ km s$^{-1}$ Mpc$^{-1}$. At all redshifts, a Milky Way type reddening law has been used to calculate the attenuation

members. Nevertheless, we can evaluate filling factors for regions of a particular transparency ($\tau_B \geq 1$, $\tau_B \geq 0.1$ etc.) using Eq. (6). For $\tau_B \geq 1$, for example, we derive an effective cross-section of $180 \times 21\pi$ kpc$^2$ for 180 spiral disks randomly orientated in the cluster. The total surface area of Virgo is 4.4 $10^6$ kpc$^2$ implying that the probability of a line-of-sight possessing an optical depth greater than unity is $P(\tau_B \geq 1.0) \simeq 0.3\%$. In a similar fashion, we derive a probability of only 3% for a line-of-sight with $\tau_B \geq 0.1$.

The low optical depths we derive for the intra-cluster medium (ICM) are apparently incompatible with the paucity of QSOs detected behind nearby clusters (Boyle et al. 1988; Romani & Maoz 1992). These latter observations imply $\tau_B = 0.2$ over most of the ICM and, for the central 2 Mpc of Virgo for example, suggest an integrated dust mass of 4 $10^{11}$ $M_\odot$. We cannot easily account for such a large dust mass even if we sum up all the grain material expected to reside in the 180 spirals catalogued by Sandage (5 $10^9$ $M_\odot$). This may indicate that galaxies were much more prodigious sources of dust in the past and such grain material has found its way into the ICM through ram-stripping, tidal interactions and/or starburst superwinds (notably, the ratio of X-ray gas to dust in Virgo is ∼100; Schindler et al. 1999). However, current efforts to model the chemical evolution of galactic disks persuade us that present-day spirals have retained a large fraction of the dust they have produced (Edmunds & Eales 1998). Conceivably, the material responsible for QSO occlusion may originate from a hitherto unidentified abundance of low surface brightness galaxies or a large number of stars populating the ICM itself (Ferguson et al. 1998).

*Acknowledgements.* We thank Iain Coulson for his assistance in taking the SCUBA observations. We appreciate the generosity of Michele Thornley and Bob Sanders who, respectively, made BIMA SONG and HI measurements available to us. PBA acknowledges the continued financial support of PPARC and the award of a study grant by the Royal Society to visit France. Je remercie James Lequeux et Françoise Combes qui m'ont acceuilli pendant deux mois à l'Observatoire de Paris.

## References

Abraham, R., Tanvir, N., Santiago, B., et al. 1996, MNRAS, 279, L47
Agladze, N., Sievers, A., Jones, S., Burlitch, J., & Beckwith, S. 1994, Nature, 372, 243
Alton, P., Trewhella, M., Davies, J., et al. 1998a, A&A, 335, 807 (ATD)
Alton, P., Bianchi, S., Rand, R., et al. 1998b, ApJ, 507, L125
Alton, P., Xilouris, E., Bianchi, S., Davies, J., & Kylafis, N. 2000, A&A, 356, 795
Andre, P., Ward-Thompson, D., & Barsony, M. 1993, ApJ, 406, 122
Beckman, J., Peletier, R., Knapen, J., Corradi, R., & Gentet, L. 1996, ApJ, 467, 175
Begemann, K., Broeils, A., & Sanders, R. 1991, MNRAS, 249, 523
Berlind, A., Quillen, A., Pogge, R., & Sellgren, K. 1997, AJ, 114, 107
Bianchi, S., Alton, P., Davies, J., & Trewhella, M. 1998, MNRAS, 298, L49
Bianchi, S. 1999, Ph.D. Thesis, University of Cardiff
Bianchi, S., Davies, J., & Alton, P. 1999, A&A, 344, L1
Bianchi, S., Davies, J., & Alton, P. 2000a, A&A, 359, 65
Bianchi, S., Ferrara, A., Davies, J., & Alton, P. 2000b, MNRAS, 311, 601
Block, D., Witt, A., Grosbol, P., Stockton, A., & Moneti, A. 1994, A&A, 288, 383
Block, D., & Greenberg, M. 1996, New Extragalactic Perspectives in the New South Africa (Kluwer)
Bohlin, R., Savage, B., & Drake, J. 1978, ApJ, 224, 132
Bosma, A. 1981, AJ, 86, 1791
Bottema, R. 1999, A&A, 348, 77
Boulanger, F., & Viallefond, F. 1992, A&A, 266, 37
Boulanger, F., Abergel, A., Bernard, J. P., et al. 1996, A&A, 312, 256
Boyle, B., Fong, R., & Shanks, T. 1998, MNRAS, 231, 897
Briggs, F., Wolfe, A., Krumm , N., & Salpeter, E. 1980, ApJ, 238, 510
Casey, S. 1991, ApJ, 371, 183
Corradi, R., Beckman, J., & Simonneau, E. 1996, MNRAS, 282, 1005
Cuillandre, J-C., Lequeux, J., Allen, R., Mellier, Y., & Bertin, E. 2000, ApJ, submitted
Churches, D. K. 1999, Ph.D. Thesis, University of Cardiff
Churches, D., Nelson, A., & Edmunds, E. 2000, MNRAS, submitted
Davies, J., & Burstein, D. 1995, The opacity of Spiral Disks, proceeding of NATO ARW, NATO Asi Ser., 469
Davies, J., Jones, H., & Trewhella, M. 1995, MNRAS, 273, 699
Désert, F., Boulanger F., & Puget, J. 1990, A&A, 237, 215
de Vaucouleurs, G., de Vaucouleurs, A., Corwin, H., et al. 1991, Third Reference Catalogue of Bright Galaxies (New York, Springer)
Disney, M., Davies, J., & Phillips, S. 1989, MNRAS, 239, 939

Dominigue, D., Keel, W., Ryder, S., & White, R. 1999, AJ, 118, 1542
Draine, B., & Lee, H. 1984, ApJ, 285, 89
Driver, S., Fernandez-Soto, A., Couch, W., et al. 1998, ApJ, 496, L93
Dunne, L. 2000, Ph.D. Thesis, University of Cardiff
Dutil, Y., & Roy, J.-R. 1999, ApJ, 516, 62
Edmunds, M., & Eales, S. 1998, MNRAS, 299, L29
Fall, M., & Pei, Y. 1993, ApJ, 402, 479
Ferguson, H., Tanvir, N., & von Hippel, T. 1998, Nature, 391, 461
Garcia-Gomez, C., & Athanassoula, E. 1991, A&AS, 89, 159
Gonzalez, R., Allen, R., Dirsch, B., et al. 1998, ApJ, 506, 152
Guélin, M., Zylka, R., Mezger, P., et al. 1993, A&A, 279, L37
Guélin, M., Zylka, R., Mezger, P., Haslam, C., & Kreysa, E. 1995, A&A, 298, L29
Heisler, J., & Ostriker, J. 1988, ApJ, 332, 543
Heraudeau, P., & Simien, F. 1996, A&AS, 118, 111
Hildebrand, R. H. 1983, QJRAS, 24, 267
Holland, W., Robson, E., Gear, W., et al. 1999, MNRAS, 303, 659
Holmberg, E. 1958, Medd Lund Obs. II, No. 13
Israel, F., van der Werf, P., & Tilanus, R. 1999, A&A, 344, L83
Issa, M., MacLaren, I., & Wolfendale, A. 1990, A&A, 236, 237
James, P., & Puxley, P. 1993, Nature, 363, 240
Jansen, R., Knapen, J., Beckman, J., Peletier, R., & Hes, R. 1994, MNRAS, 270, 373
Jenness, T. 1997, Starlink User Note 216.1
Kamphuis, J., & Briggs, F. 1992, A&A, 253, 335
Kaufer, A., Szeifert, Th., Krenzin, R., Baschek, B., & Wolf, B. 1994, A&A, 289, 740
Krumm, N., & Salpeter, E. 1979, AJ, 84, 1138
Le Bourlot, J., Pineau des Forets, G., Roueff, E., & Flower, D. 1995, A&A, 302, 870
Lequeux, J., Allen, R., & Guilloteau, S. 1993, A&A, 280, L23
Lequeux, J., Dantel-Fort, M., & Fort, B. 1995, A&A, 296, L13
Loveday, J., Peterson, B., Efstathiou, G., & Maddox, S. 1992, ApJ, 390, 338
Nelson, A., Zaritsky, D., & Cutri, R. 1998, AJ, 115, 2273
Neininger, N., Guélin, M., Garcia-Burillo, S., et al. 1996, A&A, 310, 725
Madau, P., Ferguson, H., Dickinson, M., et al. 1996, MNRAS, 283, 1388
Maloney, P. 1990, in Interstellar Medium of Galaxies ed. H. Thronson, & J. Shull
Masci, F., & Webster, R. 1999, MNRAS, 305, 937
Masi, S., Aquilini, E., Boscaleri, A., et al. 1995, ApJ, 452, 253
Mathis, J., Mezger, P., & Panagia, N. 1983, A&A, 128, 212
Mathis, J., & Whiffen, G. 1989, ApJ, 341, 808
Oey, M., & Kennicutt, R. 1993, ApJ, 411, 137
Ossenkopf, V., & Henning, Th. 1994, A&A, 291, 943
Pascarelle, S., Windhorst, R., Keel, W., & Odewahn, S. 1996, Nature, 383, 45
Peletier, R., Valentijn, E., Moorwood, A., & Freundling, W., A&A, 108, 621
Reach, W., Dwek, E., Fixsen, D., et al. 1995, ApJ, 451, 188
Regan, M., et al. 2000, in preparation
Rifatto, A., Longo, G., & Capaccioli, M. 1995, A&AS, 114, 527
Rengarajan, T. 1984, A&A, 140, 213
Romani, R., & Maoz, D. 1992, ApJ, 386, 36
Rots, A., Crane, P., Bosma, A., Athanassoula, E., & van der Hulst, J. 1990, AJ, 100, 387
Ryder, S., Staveley-Smith, L., Malin, D., & Walsh, W. 1995, AJ, 109, 1592
Sandage A., Bingelli, B., & Tammann, G. 1985, AJ, 90, 395
Schindler, S., Binggeli, B., & Boehringer, H. 1999, A&A, 343, 420
Shostak, G., Allen, R., & Sullivan, W. 1984, A&A, 139, 15
Siebenmorgen, R., Kruegel, E., & Chini, R. 1999, A&A, 351, 495
Sofue, Y., Honma, M., & Arimoto, N. 1995, A&A, 296, 33
Soifer, B., Sanders, D., Madore, B., et al. 1987, ApJ, 320, 238
Sopka, R., Hildebrand, R., Jaffe, D., et al. 1985, ApJ, 294, 242
Tacconi, L., & Young, J. 1986, ApJ, 308, 600
Terndrup, D., Davies, R., Frogel, J., Depoy, D., & Wells, L. 1994, ApJ, 432, 518
Tilanus, R., & Allen, R. 1991, A&A, 244, 8
Tilanus, R., & Allen, R. 1993, A&A, 274, 707
Tosaki, T., & Shioya, Y. 1997, ApJ, 484, 664
Trewhella, M. 1998a, MNRAS, 297, 807
Trewhella, M. 1998b, Ph.D. Thesis, University of Cardiff
Valentijn, E. 1990, Nature, 346, 153
Valentijn E., & van der Werf, P. 1999, ApJ, 522, L29
Vila-Costas, M., & Edmunds, M. 1992, MNRAS, 259, 121
Wevers, B., van der Kruit, P., & Allen, R. 1986, A&AS, 66, 505
White, R., & Keel, W. 1992, Nature, 359, 129
White, R., Keel, W., & Conselice, C. 1996, in New Extragalactic Perspectives in the New South Africa, ed. D. Block, & M. Greenberg (Kluwer)
Whittet, D. 1992, Dust in the Galactic Environment (IOP Publishing)
Williams, D., & Taylor, S. 1996, QJRAS, 37, 565
Xilouris, E., Alton, P., Davies, J., et al. 1998, A&A, 331, 894
Xilouris, E., Byun, Y., Kylafis, N., Paleologou, E., & Papamastorakis, J. 1999, A&A, 344, 868
Xu, C., & Helou, G. 1996, ApJ, 456, 163
Xu, C., Buat, V., Boselli, A., & Gavazzi, G. 1997, A&A, 324, 32
Young, J., & Scoville, N. 1982, ApJ, 260, L41
Zaritsky, D. 1994, AJ, 108, 1619
Zaritsky, D., Kennicutt, R., & Huchra, J. 1994, ApJ, 420, 87